Improving collimation of optical flux emission from scintillator crystals

Contact: jesel.patel@stfc.ac.uk

J.K. Patel
Loughborough University, LE11 3UE, United Kingdom.

D. Neely, C. D. Armstrong
Central Laser Facility, STFC, OX11 0QX, United Kingdom.

R.J. Clarke
Central Laser Facility, STFC, OX11 0QX, United Kingdom.

1 Introduction

A linear array of scintillator crystals can be used to characterise a hard X-ray spectum [1, 2]. Reflective PTFE wrapping of individual crystals improves the incident signal onto a lens coupled detector. Increasing the collimation of scintillator emission will enable further improved yield in the angular range close to the normal to the front crystal face, for better quality electron temperature measurements on laser-plasma experiments. Investigation of the impact that the surface finish and width of scintillator crystals has on the angular flux distribution, with and without PTFE wrapping, is reported here.

Using the phosphorescence of $Lu_{1.8}Y_{0.2}SiO_5 : Ce$[1] (henceforth, LYSO) reported by A. Dasgupta et al. [3], it is shown that crystals with unpolished surfaces offer increased collimation of optical emission. Absolute measurements with scintillation radioluminescence via a ^{22}Na X-ray source validates this result. Flux is observed to increase by $\sim 20\%$ in the region $\phi = 0° \pm 30°$ where ϕ is the angle to the normal to the crystal face in the x-y plane, as illustrated in Fig. 1. The Lambertian distribution is observed to approximate angular flux from crystals wrapped in PTFE, which can be used to model different imaging systems. We suggest that long timescale luminescence by UV excitation may be useful for investigation of scintillator angular emission properties without the need for exposures with radiation sources.

2 Surface finish

The angular flux distributions of 2 mm LYSO crystals with four combinations of polished and rough surfaces are plotted in Fig. 2, for both the condition that they are wrapped only in black anodised aluminium foil (henceforth referred to as 'unwrapped'), and for the condition that they are wrapped in 0.4 mm of reflective PTFE tape (henceforth, 'PTFE wrapped'). Full-width half-maxima (FWHM) of these plots are plotted in Fig. 3, where the error bars of the angular FWHM are

$$\delta_{\mathrm{FWHM}} = \pm\sqrt{5° + 5° = 10°} \approx \pm 3.2°$$

to 2 significant figures, where 5° is the smallest angular interval between flux measurements. Figs. 3 and 2 illustrate the significantly improved collimation of radiance from crystals with unpolished surfaces, which is as large as a 100° decrease in FWHM with unwrapped scintillators. The effect is less pronounced when crystals are PTFE wrapped, but unpolished crystals, and especially those with only the front and rear 2×12 mm faces polished, still show significantly improved collimation compared with those which have all faces polished. Notably, 'all faces polished' crystals have a broader flux profile than a diffuse Lambertian emitter, shown in black in Fig. 2. The Lambertian model for a diffuse source, is given by

$$I(\phi) = I_0 \cos\phi,$$

where $I(\phi)$ is the radiant flux at ϕ, the angle to normal indicated by the x-axis in Fig. 1, and I_0 is the radiant flux when $\phi = 0°$. Crystals with just one or no polished faces closely follow such a distribution when PTFE wrapped.

The 'all faces polished' crystal has a similar FWHM when wrapped in PTFE (red plot, Fig. 2 (right)) as

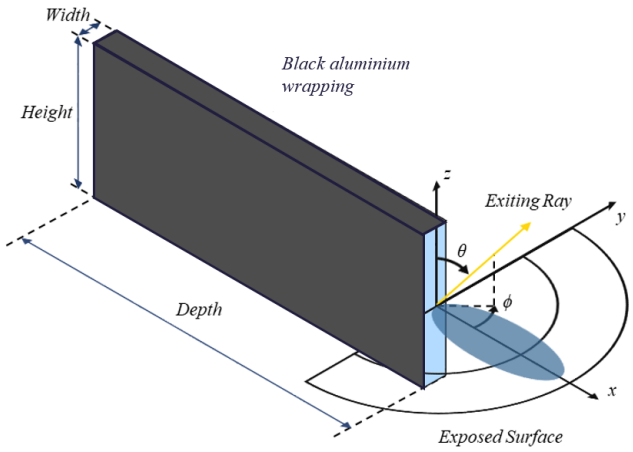

Figure 1: Crystal schematic showing the angle, ϕ, between the normal to the exposed front face and the line to the center of the camera sensor, which is varied. Anodised aluminium wrapping was used to prevent light transmitted from the other faces from falling on the sensor. Crystal depth and height dimensions used were 30×12 mm, and the widths were varied between 1, 2 and 5 mm. Image edited from J. Davies, 2019 [4].

[1] read 'cerium doped lutetium-yttrium oxyorthosilicate'

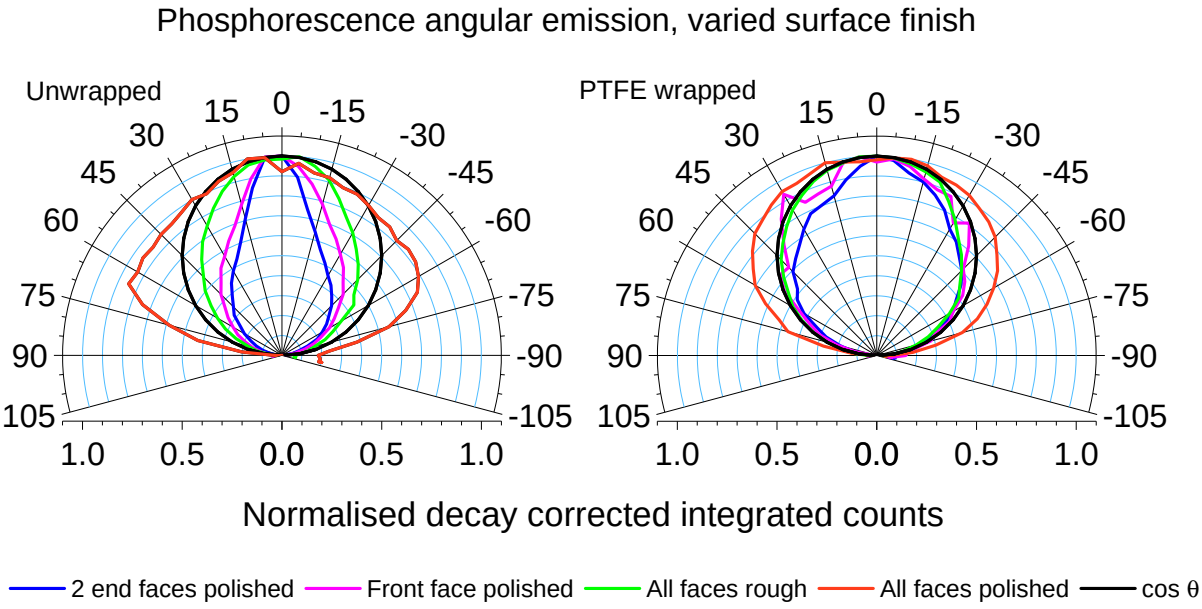

Figure 2: Normalised angular emission for unwrapped (left) and PTFE wrapped (right) crystals with different surface finishes.

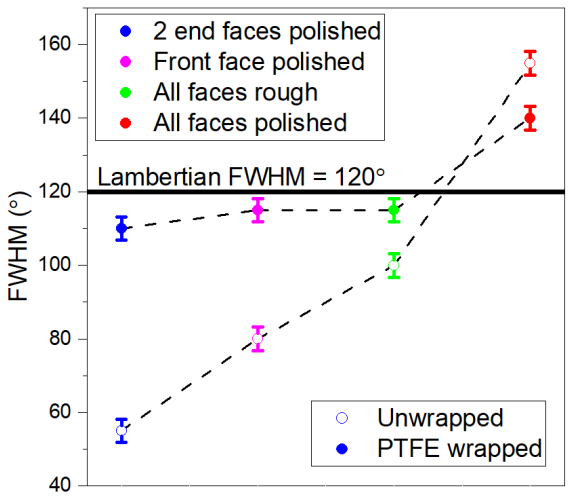

Figure 3: FWHM for each surface finish, with and without PTFE wrapping.

when it is not wrapped, despite the distribution clearly more closely resembling the Lambertian. This suggests that the broad, flat angular profile of the unwrapped crystal (red plot, Fig. 2 (left)) may be explained by an increased probability of transmission of rays through the back face of the crystal for a polished crystal with no additional reflective wrapping.

3 Crystal width

Fig. 4 shows the effect of changing the width of 'all faces polished' crystals on the angular flux distribution, for the unwrapped (top) and the PTFE wrapped (bottom) cases. When PTFE wrapped, all crystal widths produce angular flux profiles closely resembling a diffuse Lambertian cosine emitter, with only the 5 mm crystal showing a significantly different FWHM at 130°, compared with the 120° FWHM of a Lambertian.

In the unwrapped case the 1mm and 2mm crystals show similar relative depletion of flux at angles within $\pm 70°$ of $\phi = 0°$, as was seen in the surface finish measurements in §2. Sharp features in the flux profile are likely due to inconsistency of internal reflectivity of the back face; a result of crystal imperfections or scratches in the anodised aluminium wrapping. However, these losses are reduced or removed in the 5mm crystal's angular distribution, where the increased width may reduce the proportion of rays which are incident on the back face of the crystal at angles steeper than the critical angle ($\theta_C \approx 30°$ for LYSO/air interface), preventing the losses seen in the thinner crystals. As illustrated by the bottom plots in Fig. 4, these losses are also reduced by the reflective PTFE wrapping, which produces distributions which closely resemble Lambertian cosines for each of the different crystal widths.

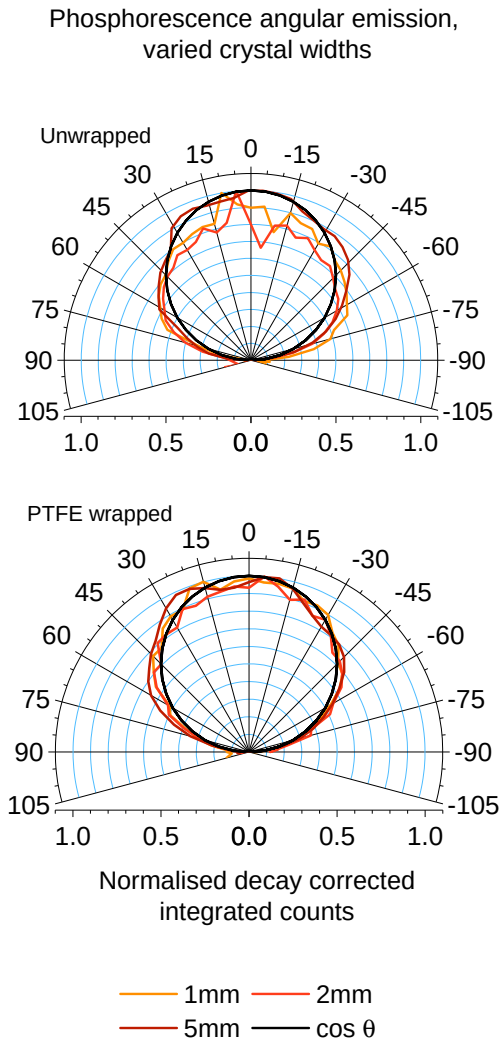

Figure 4: Normalised angular emission for unwrapped (top) and PTFE wrapped (bottom) crystals with different widths.

Table 1: Full-width-half-maxima and total light yield[a] for angular flux distributions of crystals scintillating with the ^{22}Na source.

Crystal width, polished surfaces	FWHM (°)	Total light yield ($\times 10^6$ counts)
2mm, 2 end faces	115	36.4
2mm, all	150	36.5
5mm, all	135	114.3

[a] calculated by summing integrated counts through angles $\phi = 0° \pm 90$ °.

4 Angular emission with Na-22 source

Absolute measurements using a radioactive Na-22 source to cause scintillation, rather than phosphorescence, confirm that collimation of the crystal light emission with the 2 front and rear polished surfaces increases the normal ($\phi = 0°$) light yield by $\sim 30\%$, compared with a crystal with all faces polished (see Fig. 5). Total light yield from the two 2mm crystals was comparable, but the large 5mm crystal produced a yield of ≈ 3.1 times that of the 2mm crystals. The FWHM of the radioluminescence angular distributions with the phosphorescence measurements agree to within the $\pm 3.2°$ error of one another.

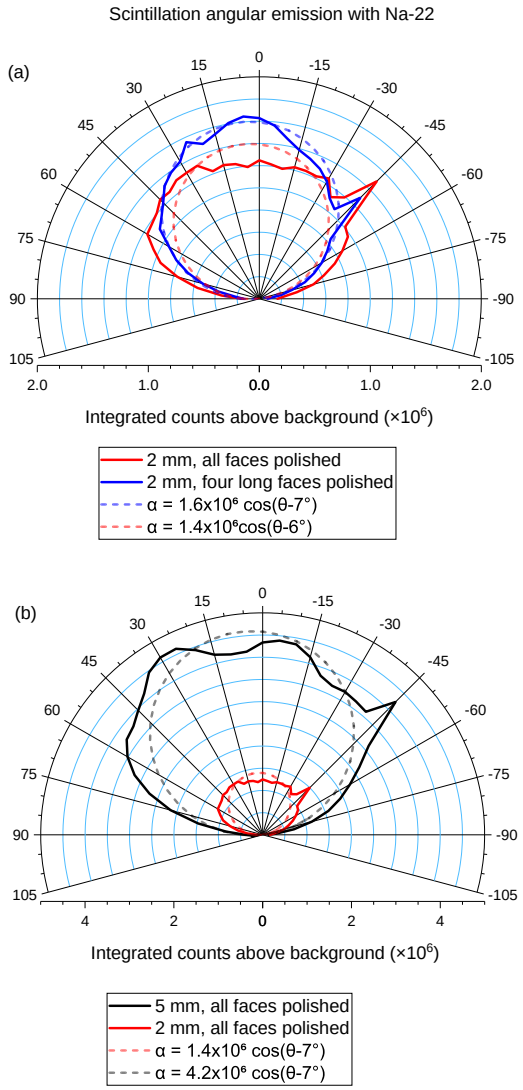

Figure 5: Angular emission of crystals with (a) different surface finishes, and (b) different crystal widths. Spikes in signal at 45° are suspected to be a result of a light leakage reflecting from the front face of the crystal onto the camera. Dashed lines are Lambertian profiles plotted to guide the eye.

5 Conclusion

The agreement between phosphorescence and scintillation angular flux distributions supports the notion that properties of optical emissions from scintillators can be effectively investigated with scintillator luminescence not requiring ionizing radiation. Other potential non-destructive luminescence mechanisms which might be useful for appropriate scintillators are: electro- (applying an electric field across a scintillator); piezo- (application of mechanical stress); thermo- (heating); and sono- (sonic driven gas cavity collapse in liquids) luminescence.

PTFE wrapped crystals with some unpolished surfaces have angular flux distributions which can be modelled reasonably well by a Lambertian distribution. However, some significant collimation of optical emissions from scintillator crystals is achieved by using crystals with surfaces parallel to the line of sight of the scintillation imaging camera unpolished. Future iterations of the attenuation based X-ray spectrometer developed at the CLF will take this into account to improve the resolution of electron temperatures in laser-plasma diagnosis.

6 Appendix A - Technical procedure

The following set-up and procedure were constructed on to measure the optical flux emitted from the front face of the scintillator crystals, through the angles $\pm 90°$ to the normal of the crystal face, as shown in Fig. 6. Isolation of the flux through the front face of the crystal was achieved by wrapping the other faces with anodised aluminium, and the controlled variation of the angle to the normal was executed by the rotation of the crystal relative to the EMCCD camera sensor with a motorized rotating stage (again, see Fig. 6).

Equipment list

- LYSO crystal batches from Epic-Crystal, all with length and height dimensions 30mm × 12mm:
    1. Four 2 mm width crystals with different surface finishes: all surfaces polished (×1); both 12 × 2 mm end faces polished, with remaining four faces along the length rough (×1); single 12 × 2 mm front face polished, with remaining five faces rough (×1); and all faces rough (×1).
    2. 3 × all faces polished crystals with different widths: 1 mm, 2 mm and 5 mm.
- Andor iXon EMCCD camera, used with a computer with the appropriate graphics network card installed.
  Model no.: DU-888E-C00-#BV.
- NAVITAR 25 mm F0.95 lens.
- 0.5 mm lens spacer
- Thorlabs Elliptec motorized rotating stage and interface board. Part no.: ELL18K/M
- Anodised aluminium foil for lining of light tight cardboard box, and masking of luminescent electrical components on the rotating stage circuitry
- 380 nm UV LED.
- SRS digital pulse generator. Part no.: DG645.

Hardware set-up

The EMCCD camera was set up with the 0.5 mm lens spacer and 25 mm F0.95 lens and placed outside the light tight box to prevent overheating and fire hazard from the camera's cooling system. A 25 mm diameter hole in the side of the box allowed the end of the lens to be placed in the light tight environment, opposite the centre of the rotating stage at around 25 cm, such that the distance from the centre of the stage to the EMCCD was $\approx$ 28 cm. Cooling the camera to -40 °C and using the Andor SOLIS software to take some test acquisitions with **EM gain disabled** and 1 ms exposures, the rotating stage and interface board were observed to be luminescent in places. Anodised aluminium was therefore used to mask these features, and the exposure time increased until 10s single shot acquisitions produced a smooth background noise.[2] Fixing the exposure time at 10s, the process was repeated with EM gain enabled, increasing by increments of 20 and ensuring no light leakage or circuit luminescence was observed until smooth background images could be reliably achieved with EM gain set to the maximum 300. Additional aluminium wrapping on the rotational stage was also adjusted to ensure that it did not contact with the piezoelectric motors or their tracks, and that unimpeded 360°capability was maintained, by 'jogging' the stage through a full rotation using the Thorlabs ELLIPTEC accompanying software. Anodised aluminium was also used to create a window over the camera lens, reducing the horizontal aperture to 10 mm while maintaining the full 25mm vertical aperture height, as shown schematically in Fig. 6 (inset). By constraining the solid angle of the optical emissions, the angular error in each measurement is limited to $\delta_\phi = \pm 1.6°$, where the subscript distinguishes the error in measurements at each angle, ϕ, from the error in the FWHM values calculated in §2.

Software set-up

Sequences of 5° 'jog' steps were constructed in the ELLIPTEC software, for 40 'forwards' (clockwise) and 40

[2]Note: Andor SOLIS users should ensure that the scaling of the image is appropriate if expected features or noise are not initially displayed. Settings are by default loaded from the last session. The 'plot Data Histogram' feature under 'Display' (also available by right-clicking on the acquisition in question) is particularly useful for checking and adjusting this.

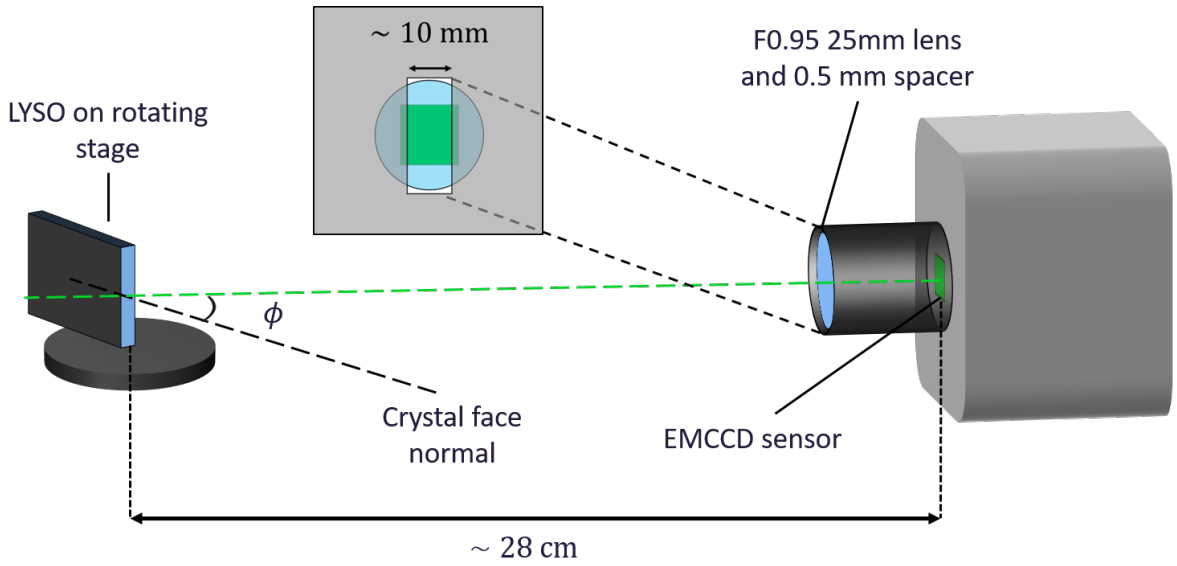

Figure 6: Angular flux measurement set-up schematic. The LYSO is rotated through an angle $-100° \leq \phi \leq 100°$. Inset shows the anodised aluminium window over the camera lens used to constrain angular uncertainty in measurements. Not to scale.

'backwards' (anti-clockwise) steps, such that execution of the sequence rotated the stage clockwise through 100° and then back through -100° to the original position, in 80 5° steps. The time delay between each step could be varied such that rotation steps were implemented between camera acquisitions, so two sequences were constructed for 1s exposures and 5s exposures. To obtain a series of exposures for each angular position, the 'kinetic' acquisition mode in the SOLIS software was used, allowing a series of 86 exposures of a set time to be taken with a 5s delay between them, allowing period for the stage to rotate the crystal to the next position.

Data acquisition procedure

For each of the four 2mm crystals, the following procedure was carried out to collect the angular flux distribution data.

1. **Crystal pumping:** The selected crystal was 'pumped' while unwrapped with the UV LED, by setting it on the stage around 20cm from the LED with a 12mm× 30mm face perpendicular to the line-of-sight of the LED, and irradiated for 15s as set by the pulse delay generator, before flipping over so that the opposite large face was exposed for the same period. The light tight box was sealed between pumping to prevent eye damage from the UV light. The crystal was then wrapped in anodised aluminium foil, taking care to not split or scratch the foil on the crystal edges and vertices, folding it to prevent contact between crystal surface and a cut edge of the foil, where the uncoated reflective aluminium is exposed. Care was also taken to prevent wrapping overhanging the edges of the front face to prevent unintended extinguishing of radiance at angles approaching $\phi = 90°$.

2. **Alignment:** The crystal was then clamped in place on the stage, such that the plane of the exposed front face is close to (< 1 mm) passing through the diameter of the stage which is perpendicular to the normal of the crystal face. Using 0.01s, EM gain disabled, room-lit video acquisitions, the crystal was then aligned such that it was face-on to the camera, rotating by incrementally smaller steps until the sides of the crystal were minimised, as well as using the inside back edges of the crystal to check that $\phi = 0°$, to within 0.5°. Then it was rotated 'backwards' 100°, the light tight box closed, and the acquisition settings adjusted for a kinetic series of 86× 5 s exposures with EM gain enabled and set at 300.

3. **Acquisition:** After allowing ~ 6 mins to pass after initial UV pumping to allow the fast component of the observed phosphorescence decay detailed in §7, acquisition was initiated. After the first 3 exposures, the 80 step, ±100° ELLIPTEC rotation sequence was executed. When the acquisition was complete, the pixel co-ordinates of a region of interest (ROI) which contained the image of the front face of the crystal in all of the 40 angular positions were identified, and an Andor Basic program written by the author was used to extract the number of integrated counts and associated standard error in the ROI for each of the 16-bit frames of the 86 frame series.

4. **PTFE wrapping:** The aluminium wrapping of the crystal was then removed, and ≈0.4mm of PTFE tape was used to wrap the five unexposed faces, before it was again wrapped in anodised aluminium, and steps 2 and 3 were repeated.

For the three all-faces-polished crystals of different widths a similar procedure was used, however, the 'pumping' was carried out before every acquisition, after the crystals were wrapped, and the crystals were instead pumped through the exposed 12 mm×2 mm front face. This batch of crystals seemed to radiate with flux around an order of magnitude greater than the 2mm crystal batch, so acquisitions could also be carried out with shorter 1s exposures to reduce the impact of the decay described in §7.

Scintillation emission measurements were taken via the same procedure, but all crystals were PTFE wrapped from the beginning, and a ^{22}Na radioactive source was clamped at ≈ 15 cm from the crystal positions of the stage. Lead bricks were used to shield the camera from direct line of sight of the source. The ^{22}Na source maintained the same position throughout the acquisitions and changes between crystals.

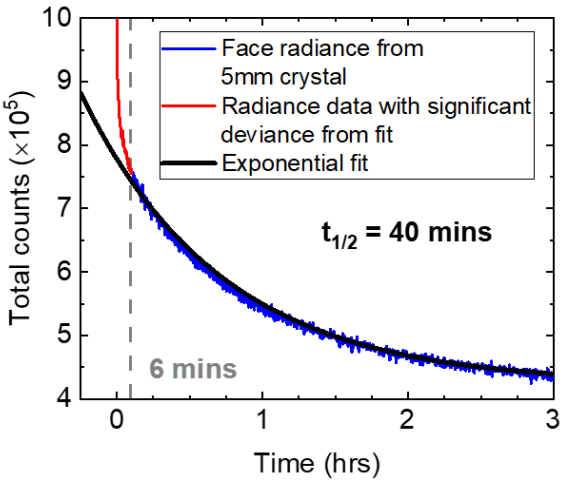

Figure 7: Phosphorescent radiance from the front face of a 5mm LYSO crystal over 3 hours after a 10s 380nm face-on LED pulse, showing region of fast decay, deviating from exponential fit at $t < 6$ minutes after end of pumping pulse.

7 Appendix B - LYSO phosphorescence

A. Dasgupta *et al.* [3] reported that the LYSO absorption line at 363nm leads to a phosphorescence with a ∼ 54 min decay half-life. The reported results in §2 and §3 used this property by 'pumping' crystals with a 380nm LED to trigger the optical phosphorescence emission. A single measurement recording cycle took between 5 and 8 minutes (depending on camera exposure time required), which is a significant fraction of LYSO's half life. Hence, the time interval between measurements were also recorded, so that an approximate exponential function could be subtracted from each angular series.

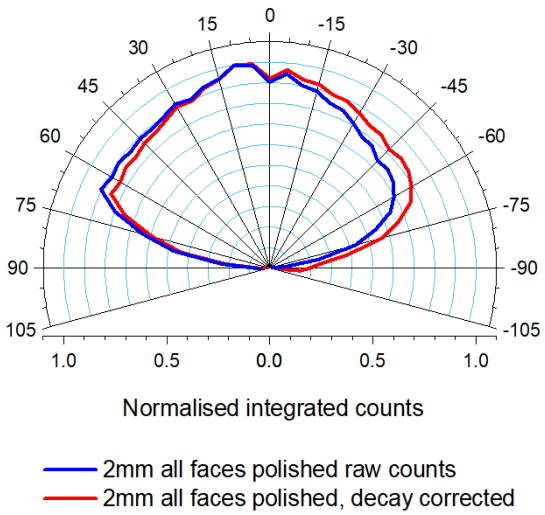

Figure 8: Angular radiance of unwrapped 2mm crystal with all faces polished, before (blue) and after (red) correcting for approximated exponential decay. Correction restores some symmetry lost as radiance decays during rotation from 100° through -100°.

References

[1] D. Rusby *Novel scintillator-based x-ray spectrometer for use on high repetition laser plasma interaction experiments* Rev. Sci. Instrum. 89, 073502 (2018); `https://doi.org/10.1063/1.5019213`, 2018.

[2] C. D. Armstrong. *Bremsstrahlung radiation and fast electron transport in laser-plasma interactions.* Ch. 4.3.2. PhD thesis, University of Strathclyde, 2019.

[3] A. Dasgupta *et al. Calibrating LYSO crystals as part of a hard X-ray spectrometer* CLF Annual Report, 2019.

[4] J. Davies *Investigating the angular flux distribution from LYSO scintillators.* Imperial College London, 2019.